Spectroscopic study of stimulated Brillouin scattering

John J. Turechek[a] and F. F. Chen

Electrical Sciences and Engineering Department, University of California, Los Angeles, California 90024
(Received 7 April 1980; accepted 13 March 1981)

Results are summarized of a diagnostic study of underdense plasma targets, leading to the first observation of stimulated Brillouin scattering arising from thermal-level fluctuations. Included are; (1) a detailed analysis of spectroscopic measurements of the plasma before and during laser heating, (2) computer calculations of plasma evolution during the laser pulse, (3) observations and anlaysis of Brillouin scatter, and (4) spectroscopic observations of forbidden satellite line emission during Brillouin scatter.

I. INTRODUCTION

When intense electromagnetic waves impinge on a plasma, various parametric processes have long been known to occur near the resonance layer where the wave frequency ω_0 matches the plasma frequency ω_p. These lead to enhanced absorption via mechanisms such as the parametric decay and oscillating two-stream[1] instabilities and resonance absorption.[2] It was later realized, however, that parametric instabilities could occur in the underdense layers, where $\omega_p < \omega_0$, and that these could cause anomalous reflection of laser light, preventing it from reaching the absorption layers. The two most widely studied instabilities are stimulated Brillouin scattering, in which the incident light wave decays into an ion acoustic wave and a backscattered light wave, and stimulated Raman scattering in which it decays into an electron plasma wave and a backscattered or sidescattered wave. Theoretical predictions[3-5] showed, surprisingly, that stimulated Brillouin scattering had a lower threshold than stimulated Raman scattering in spite of Manley–Rowe considerations which would lead one to expect that conversion to the higher-frequency plasma wave would be more efficient than to the lower-frequency ion wave. The reasons apparently have to do with differences in damping, speed of convection of wave energy from the pump zone, and sensitivity to density gradients. Furthermore, computations of the nonlinear behavior[6] show stimulated Brillouin scattering to be more dangerous than stimulated Raman scattering because of a higher saturation amplitude.

The present experiment was conceived to verify the basic linear theory of stimulated Brillouin scattering. Although backscattering has been seen in many solid-target experiments,[7] the nonuniform, expanding plasmas created by the laser unnecessarily complicate the observations. We employed a large plasma target created separately by a high-current arc and achieved the requisite intensity with a CO_2 laser. Since the publication of our preliminary results,[8] other groups[9,10] have also detected stimulated Brillouin scattering from a gaseous target. However, these plasmas were laser-created and contained a high level of initial acoustic turbulence. In the work reported here, stimulated Brillouin scattering was observed to arise from thermal noise.[11]

This investigation is relevant to both magnetic fusion in long solenoids[12] and to inertial fusion in pellet implosions.[13] In the case of long solenoids with plasma heating by long-pulse CO_2 lasers, the beam is spread both in space and in time compared with the pellet case, and peak intensities of only 10^{12} W/cm^2 or below are needed under reactor conditions. However, because of the relatively long scale lengths involved, this intensity is well beyond the threshold of stimulated Brillouin scattering; and means must be found to control this instability. In the case of pellet fusion, it was originally feared[14] that parametric reflection would scale rapidly with increasing intensity and reach 100% before fusion conditions could be met. Fortunately, it was found experimentally[15] that reflection saturated at 10–20% for intensities above 10^{16} W/cm^2. This has been explained[16] by the change in plasma density and temperature profiles caused by momentum and energy deposition connected with the backscattering process. As the longer pulses and larger pellets needed for energy breakeven are approached, however, the possibility of parametric backscatter again becomes worrisome[13]; indeed, it has been found[17] that the structured pulses required for ablative pusher implosions, as simulated by a prepulse, would greatly increase the anomalous reflection. Computer predictions of pellet performance must now include parametric effects, and experiments of this type serve to establish a level of confidence in the relevance of the basic theory.

II. THEORETICAL BACKGROUND

A. Results on stimulated Brillouin scattering

The theory of parametric instabilities in a homogeneous plasma has been worked out in great detail.[4,5] A simple physical derivation of stimulated Brillouin scattering applicable to the most virulent case, namely, when the scattered wave is polarized in the same plane as the incident wave and propagates in the opposite direction, is given by Chen.[18] The intrinsic growth rate in a homogeneous plasma is given by

$$\gamma_0 = (\hat{v}_0/2c)(\omega_0/\omega_s)^{1/2}\omega_{pi}, \tag{1}$$

where

$$\hat{v}_0^2 = (8\pi/c)(c/m\omega_0)^2 I_0, \tag{2}$$

[a] Present address: Ultra-Violet Products, Inc., San Gabriel, Calif. 91778.

 0031-9171/81/061126-16$00.90

$$\omega_s \simeq 2k_0 c_s, \tag{3}$$

$$c_s^2 = (ZkT_e + 3kT_i)/M, \tag{4}$$

$$\omega_{pi}^2 = 4\pi n_{0i} Z^2 e^2/M = 4\pi n_{0e} Ze^2/M, \tag{5}$$

c is the velocity of light, m is the mass of the electron, I_0 is the intensity of the pump wave, k is the Boltzmann constant, Z is the charge number of the ions, n_{0i} and n_{0e} are the equilibrium ion and electron densities, respectively, and the other symbols are standard.

The proper treatment of an inhomogeneous plasma was pointed out by Rosenbluth and co-workers,[19,20] and the problem of finite plasmas was solved by two other groups.[21,22] Finally, the space-time evolution of the excited wave packets has also been treated.[23-25] In our experiment, finite interaction length L is more important than inhomogeneity, and ion wave damping γ_s is more important than loss of energy by convection. The physical situation, then, is as follows: A parametric Brillouin scattering instability grows in a finite region of homogeneous plasma. The ion wave hardly propagates during the interaction and loses energy primarily by ion Landau damping. The backscattered wave has negligible damping but rapidly convects energy from the interaction region. The amplitude of the backscattered wave increases in the $-\mathbf{k}_0$ direction, as usual; but the amplitude of the ion wave does not grow in the $+\mathbf{k}_0$ direction, as in the normal picture.[1] Rather, the ion wave amplitude *decreases* in the $+\mathbf{k}_0$ direction because the pondermotive driving force depends on the amplitude of the scattered wave, and the ion waves do not have any appreciable convection. Under these conditions, the backscatter intensity is given by[18,21]

$$I_2 = I_n \exp(2\gamma_0^2 L/c\gamma_s), \tag{6}$$

where I_n is the intensity of the initial noise from which the backscatter grows. Equation (6) is the theoretical result that this experiment is designed to check.

B. Plasma heating

In underdense plasmas, absorption of the laser light occurs through classical collisional damping of the light wave (inverse bremsstrahlung). The classical absorption coefficient varies as n^2, while the pondermotive force that drives parametric instabilities varies as n. For this reason, microwave experiments, which have low ω_0^2 and hence low $\omega_p^2 \propto n$, can be designed to test pure parametric effects without plasma heating; but laser experiments, which have higher ω_0^2 and hence higher n, almost always have heating effects convolved with parametric phenomena.[11] We therefore summarize the absorption results pertinent to this experiment; an extensive literature on laser heating exists in connection with magnetic confinement in long linear solenoids.[26]

The focal region in which this experiment is performed has the approximate shape of a cylinder 1 mm in diameter and several cm long. The laser is fired into a target plasma created by an arc discharge, typically in 7 Torr of He. Although the initial conditions are $n_e \simeq 5\times10^{16}$ cm^{-3} and $kT_e \simeq 4$ eV, the laser pulse rapidly completes the ionization of the neutral gas, bringing n_e to $\simeq 4\times10^{17}$ cm^{-3}, and heats the plasma to a much higher temperature, which we wish to estimate.

The high-frequency absorption coefficient α is given by[27]

$$\alpha = 3.08\times10^{-7} Z n_e^2 \ln\Lambda(\omega) T_{ev}^{-3/2} \omega_0^{-2} (1 - \omega_p^2/\omega_0^2)^{-1/2} \text{ cm}^{-1}, \tag{7}$$

where $\ln\Lambda(\omega)$ is a frequency-dependent Coulomb logarithm. For $\omega = \omega_0 = 1.78\times10^{14}$ sec^{-1}, corresponding to 10.6 μm radiation, Λ is approximately[28]

$$\Lambda(\omega) \simeq 2.2 T_{ev}^{3/2}/Z. \tag{8}$$

Z is the ionic charge number, and T_{ev} is the electron temperature in eV. For the underdense plasmas used here, we neglect the dielectric correction $(1 - \omega_p^2/\omega_0^2)^{-1/2}$ in Eq. (7). The local deposition of heat is $Q = \alpha I_0$. Evaluating α for 10.6 μm light, we obtain

$$Q = 9.7\times10^{15} Z \ln\Lambda(\omega) n_{17}^2 T_{ev}^{-3/2} I_{10} \text{ erg/cm}^3 \text{ sec}, \tag{9}$$

where n_{17} is electron density in units of 10^{17} cm^{-3} and I_{10} is laser intensity in units of 10^{10} W/cm^2.

Since the heated region is long and slim, radial heat conduction away from the beam axis determines T_e through the heat equation

$$\frac{\partial}{\partial t}(\tfrac{3}{2} n_e k T_e) + \nabla \cdot \mathbf{q}_e = Q. \tag{10}$$

The heat flux is given by[29]

$$\mathbf{q}_e = -3.16(n_e kT_e/m\nu_{ei}) \nabla kT_e \equiv -\kappa_e \nabla T_{ev} \text{ erg/cm}^2 \text{ sec}. \tag{11}$$

The electron-ion collision frequency ν_{ei} is

$$\nu_{ei} \simeq 2.9\times10^{-6} Z \ln\Lambda\, n_e T_{ev}^{-3/2}. \tag{12}$$

For heat conduction, the low-frequency value of Λ, about one-fourth the value given by Spitzer,[30] is to be used here.[28] The coefficient of thermal conductivity is then given by

$$\kappa_e = 3.1\times10^9 T_{ev}^{5/2}/Z \ln\Lambda \text{ erg/cm sec eV}. \tag{13}$$

With these values, Eq. (10) can be written

$$2.4\times10^5 \frac{\partial}{\partial t}(n_{17} T_{ev}) - \frac{3.1\times10^9}{Z \ln\Lambda} \nabla \cdot (T_{ev}^{5/2} \nabla T_{ev}) = 9.7\times10^{15} Z \ln\Lambda(\omega) n_{17}^2 I_{10} T_{ev}^{-3/2}. \tag{14}$$

The initial heating rate can be estimated by neglecting the conduction term. Expansion of the heated plasma will occur on the same time scale, but to obtain an estimate we may take n to be constant. Dropping the subscript on T_{ev}, we then have

$$T^{3/2} \partial T/\partial t = 4.1\times10^{10} Z \ln\Lambda(\omega) n_{17} I_{10}. \tag{15}$$

The intensity I_{10} can be approximated by a linear rise from 0 to 5 in 40 nsec:

$$I_{10} = 5t_{ns}/40. \tag{16}$$

Integrating Eq. (15) with $\ln\Lambda = 7$, we obtain

$$T^{5/2} = T_0^{5/2} + 44 Z n_{17} t_{ns}^2. \tag{17}$$

Specifically for He, where $Z = 2$, $n_{17} \simeq 4$, and $T_0 \simeq 4$ eV, this yields $T \simeq 200$ eV. Since this is well in excess of

the measured temperature at or after the peak in I_0, when the backscattering occurs, the temperature is apparently conduction limited.

We therefore compute the steady-state temperature set by radial heat conduction. In this case Eq. (14) gives

$$r^{-1}(rT^{5/2}T')' = -3.2\times10^{6}Z^{2}\ln\Lambda\ln\Lambda(\omega)n_{17}^{2}I_{10}T^{-3/2}, \tag{18}$$

where the prime indicates $\partial/\partial r$. If we assume n and I_0 to be uniform, we have

$$T^{3/2}(rT^{5/2}T')' = -Ar, \tag{19}$$

where

$$A = 1.9\times10^{8}Z^{2}n_{17}^{2}I_{10}. \tag{20}$$

We have taken $\ln\Lambda \simeq 8$, $\ln\Lambda(\omega) \simeq 7$, and hence $\ln\Lambda\ln\Lambda(\omega) \simeq 60$ for the anticipated plasma conditions. Equation (19) can be solved by dividing the heated region into two zones: For $r \lesssim b$, I_0 is finite and constant; but $b < r \lesssim a$, I_0 vanishes and, hence, $A = 0$. Between $r = b$ and $r = a$, T falls to the initial temperature T_0. In this conduction region, Eq. (19) is simply

$$rT^{5/2}T' = -B, \tag{21}$$

where B is a constant. The solution is

$$T_b^{7/2} - T_0^{7/2} = \tfrac{7}{2}B\ln(a/b). \tag{22}$$

Here, T_b is the temperature at the beam boundary $r = b$. Because b is small, the value of T on axis is only a few eV above T_b. To find the constant B, we match the heat flux at $r = b$ to the absorbed energy per unit length

$$2\pi b q_e = \pi b^2 Q. \tag{23}$$

From Eqs. (11) and (21) we have

$$q_e = -\kappa_e T' = -\kappa_e B/bT_e^{5/2}. \tag{24}$$

Equations (23), (24), (9), and (13) then yield

$$B \simeq 1.0\times10^{8}b^{2}Z^{2}n_{17}^{2}I_{10}T_b^{-3/2}. \tag{25}$$

The radius a at which T falls to the negligibly small value T_0 is not known, but it is sufficiently accurate to take $a/b = 20$, $\ln(a/b) = 3$. Equations (22) and (25) then give

$$T_b^{5} \simeq 3.2\times10^{8}Z^{2}n_{17}^{2}(\pi b^{2}I_{10}), \tag{26}$$

or

$$T_b \simeq 50Z^{2/5}n_{17}^{2/5}P_{10}^{1/5}\ \text{eV}, \tag{27}$$

where P_{10} is the laser power in units of 10^{10} W. The conduction limited temperature depends only on total power, not intensity. For typical values $Z = 2$, $n_{17} = 4$, $P_{10} = 0.05$, Eq. (27) gives $T_b \simeq 63$ eV. Thus, we may expect the arc plasma to be greatly heated by the laser during the scattering experiments.

III. DESCRIPTION OF THE EXPERIMENT

Figure 1 is a schematic representation of the experiment. The CO_2 laser chain consisted of a Lumonics model 103-1F laser oscillator with stable resonator optics followed by three homemade TEA amplifier stages of the Demanchin type, similar to those described by Marhic,[31] except that the pre-ionizer rods were encased in Plexiglass and ran transverse to the beam direction. The laser chain produced a 3.8 cm diam beam of 10.6 μm radiation with a total pulse energy of 40–50 J. Time-resolved measurements of the laser intensity indicated that approximately half the energy was contained in an initial 100-nsec gain-switched spike, with the rest appearing in a $\frac{1}{2}$ μsec tail. The laser pulses exhibited a varying amount of mode-locked modulation from shot-to-shot which appeared to be sensitive to the fine alignment of the oscillator cavity. The largest instantaneous peak powers observed in the

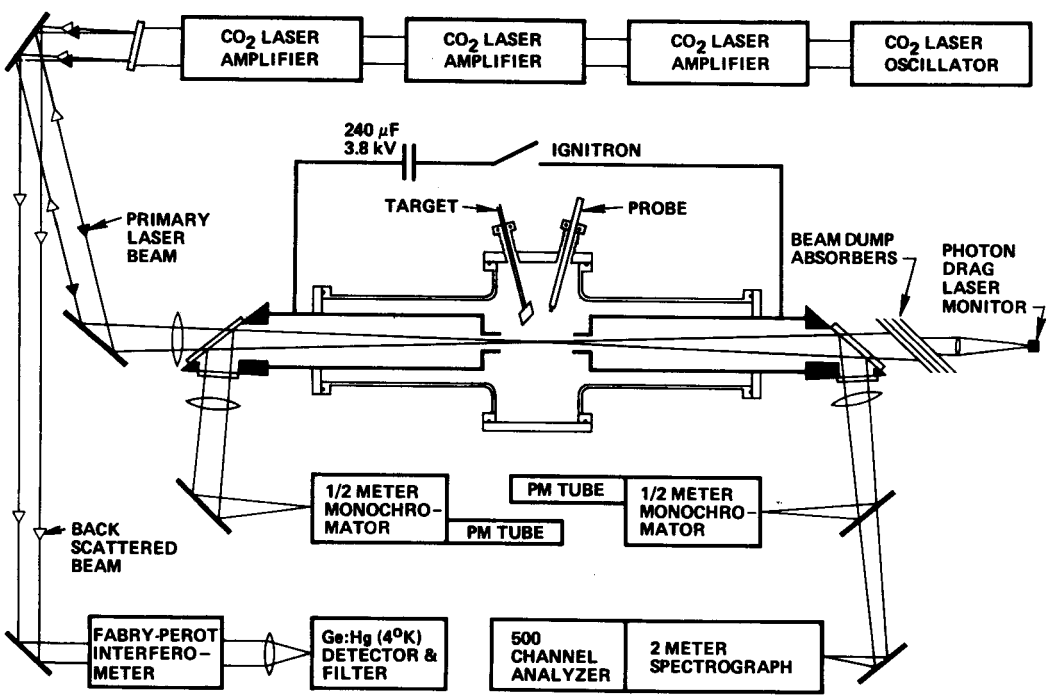

FIG. 1. Schematic diagram of the apparatus.

mode-locked pulses with a photon drag detector (400 psec rise time) and Tektronix 7904 oscilloscope (800 psec rise time) were a factor of two above the average power. Nonetheless, peak power averaged over the mode-locked pulses was reproducible to ±20% at 400 MW for those shots where no arcing occurred in the laser amplifiers. The wavelength spectrum of the output of the laser was also highly reproducible. Lasing occurred reliably on the P20 transition, with the intensity of the other components contributing less than 5%. The spectral width measured with a Fabry–Perot interferometer was 700 MHz FWHM (full width half-maximum).

The laser beam was brought to a gentle focus in the plasma by a 75 cm focal length, 7.6 cm diam, plano-convex, antireflection-coated germanium lens. A diffraction-limited focus for this optical system with an effective f number of 20 would have beam waist 0.27 mm in diameter and 1 cm in length. Measurements in the vicinity of the focus, however, indicated a much larger spot size. This is expected from lens aberrations and the highly non-Gaussian profile of the beam. The intensity distribution at the focus was measured by observing burn marks produced in polished pieces of Plexiglass with the laser beam uniformly attenuated by known amounts. The burn marks exhibited some microstructure and hot spots; however, the focus was, in general, well characterized by a 1 mm diam spot with a sharp boundary over an effective depth of focus of about 4 cm. This gave a peak intensity, averaged over the mode-locked pulses and over the focal cross section, of 5×10^{10} W/cm^2. Spillover intensities outside this region were at least two orders of magnitude lower.

Access to the plasma was provided by two-Brewster-angle NaCl windows in the vacuum chamber and two 1.27 cm diam holes in the discharge electrodes for entrance and exit of the focused beam. The Brewster-angle windows served a dual purpose: as nonreflecting windows for the laser, and as infrared-optical beam splitters for simultaneous end-on optical observation of the focal region. The exit window for the laser was backed by a stack of teflon sheets to absorb and attenuate the transmitted beam, followed by a photon drag monitor. Four ports in the vacuum chamber around the midplane of the plasma provided radial access for probes, interferometry, and spectroscopy.

The initial target plasma was created by a capacitor discharge (240 μF, 3.8 kV) between two cylindrical electrodes 2.54 cm in diameter and 10 cm apart. The discharge current was limited by approximately 1.5 μH of circuit inductance and reached a peak of 30 kA in about 30 μsec. With gas filling pressures in the range of 1–10 Torr, the plasma was thus very similar to the pulsed arc type plasma source studied extensively in Germany,[32] and elsewhere.[33] Details of the arc are given here because essentially the same plasma target was used in a series of subsequent experiments. The 10 cm gap and the cylindrically symmetric geometry were chosen to provide a uniform target plasma over the 4-cm interaction region in the focus of the laser. Detailed diagnostics of the incident and laser heated plasmas are discussed in Sec. IV. We note here, however, that for the lowest gas filling pressures (and plasma densities) backscattering was observed only at early times ($t=5$–10 μsec) during the discharge. At these early times the neutral atom density was near that of the initial filling pressure, with ionization typically on the order of 5%. The resultant evolution of the plasma in the focus of the laser was then essentially similar to laser-induced gas breakdown, but with two important differences. First, unless extraordinary precautions are taken, conventional laser breakdown in even spectroscopically pure gas is dominated by the presence of microscopic particles suspended in the gas; adequate filtering of the particles raises the breakdown thresholds to very high levels. In our particular case, no breakdown was observed in the unpre-ionized gas except for filling pressures corresponding to electron densities above the critical density n_c. Second, conventional laser breakdown is usually observed as a breakdown wave which propagates in the direction toward the laser with a typical velocity of 10^7 cm/sec, producing pronounced axial inhomogeneities.[10]

In the present experiment these difficulties were avoided by presenting to the laser a uniformly preionized incident target plasma. Typical filling pressures for the three gases used were 8 Torr for hydrogen, 7 Torr for helium, and 1.6 Torr for argon. Assuming complete outer-shell ionization for each gives electron densities of 5.2×10^{17} cm^{-3}, 4.6×10^{17} cm^{-3}, and 4.2×10^{17} cm^{-3}, respectively. Critical density for CO_2 radiation is 10^{19} cm^{-3}, so that typically we would expect $n_e \lesssim 0.05 n_c$. Spectroscopic observations revealed no axial inhomogeneities in the target arc plasma along the axis of the focal volume.

Backscattered radiation from the focal volume was recollimated by the germanium lens and directed back into the laser. This lens was tilted slightly to direct any reflections from its surfaces out of the optical path, a fact which, however, contributed to the aberration of the lens. The last NaCl window on the laser chain was slightly canted, and its inherent reflectivity (4% per surface) was used to reflect the backscattered radiation into the backscatter detection optics. The latter consisted of a large-aperture Fabry–Perot interferometer followed by a narrowband filter ($\simeq$ 10% passband) and a lens to focus the radiation onto the detector. A primary consideration in the design of the detection subsystem was the attainment of low-level backscatter sensitivity. In a backscatter experiment where elements of the detection optics are illuminated by the full intensity of the input laser beam (i.e., the collimating lens and beam splitter) the stray light levels are necessarily high. A long path length was included in the system to reduce noncollimated components of the stray light. The Fabry–Perot interferometer consisted of two 60%-reflecting standard laser output couplers mounted on an optical bench in an enclosure to minimize temperature variations from air currents. The etalon was scanned by means of a piezoelectric crystal incorporated into one of the mounts. The resulting instrument possessed only a modest finesse of about 7 but had the virtues of util-

izing the full 5 cm diam of the optics and maintaining alignment reliably over periods of several weeks.

The detector consisted of an appropriately biased mercury-doped germanium (Ge : Hg) crystal cooled to liquid helium temperature (4 °K) and loaded by 50 Ω. The sensitivity of the resulting backscatter detection was dictated by the residual stray light, equivalent to approximately 2 W (peak) at the detector or 20 W backscatter from the plasma. This corresponds to detection levels better than 10^{-7} below the input laser power. The remaining stray light nonetheless proved useful as a simultaneous monitor of the laser output for power and timing comparisons.

IV. PLASMA DIAGNOSTICS

A. Spectroscopy

Spectroscopy measurements of the plasma were taken both side-on and end-on using two $\frac{1}{2}$ m Ebert scanning monochromators fitted with S-20 response photomultiplier tubes. A 2-m spectrograph, equipped with an optical multi-channel analyzer, produced single-shot, 500-channel, high-resolution spectra for gated periods down to 100 nsec.

Electron densities in the range above 10^{16} cm^{-3} were inferred from the widths of optical emission lines. For the case of helium filling gas, widths of three He I lines (2^3S–3^3P, 3889 Å; 2^3P-4^3D, 4472 Å; and 2^3P-3^3D, 5876 Å) and one He II line ($n=3$–4, 4686 Å) were observed Theoretical density-broadened profiles and line broadening parameters were taken from Griem[34] and Cooper and Oertel[35] for the isolated lines 3889 Å and 5876 Å, and from Kepple[36] for 4686 Å. As for the allowed-forbidden combination line at 4472 Å, a detailed account of the linewidth observations in the pulsed arc, along with a discussion of the edge effect contributions, has been given by Turechek.[37]

Densities obtained from the widths of the different lines gave systematically different results with the ordering

$$n_e(3889\ \text{Å}) > n_e(5876\ \text{Å}) > n_e(4686\ \text{Å}) > n_e(4472\ \text{Å}),$$

where the ratio of the highest to lowest densities was typically about three. The effects of spatial inhomogeneities were clearly observable in the 4472 Å profiles, suggesting this mechanism as a probable cause for the rather poor agreement with theory of the observed profiles of the other He I lines. Since the average of the densities obtained from all the He I lines lay within the smaller range of error of the He II line, widths of 4686 Å were used preferentially whenever possible; this gave an estimated error of ±20% in the density.

For the other two filling gases used (hydrogen and argon) small amounts (<10% electron density contribution) of helium were added, and widths of 4686 Å were observed. Additionally, for pure hydrogen filling gas, widths of H_β ($n=2$–4, 4861 Å) were observed and compared with the calculated profiles of Griem *et al.*[38]; the resulting densities agreed within experimental error with those obtained from 4686 Å.

For linewidth measurements within the laser heated focal region, increased experimental errors associated with shot-to-shot irreproducibility and the transient character of the plasma were roughly canceled by the greater accuracy associated within the larger linewidths observed. Because of the relatively good agreement between the observed and theoretical profiles, we ascribe an accuracy of ±20% to these density measurements as well. The optical multichannel analyzer proved to be particularly powerful for these measurements. Widths of 4686 Å were used in all cases.

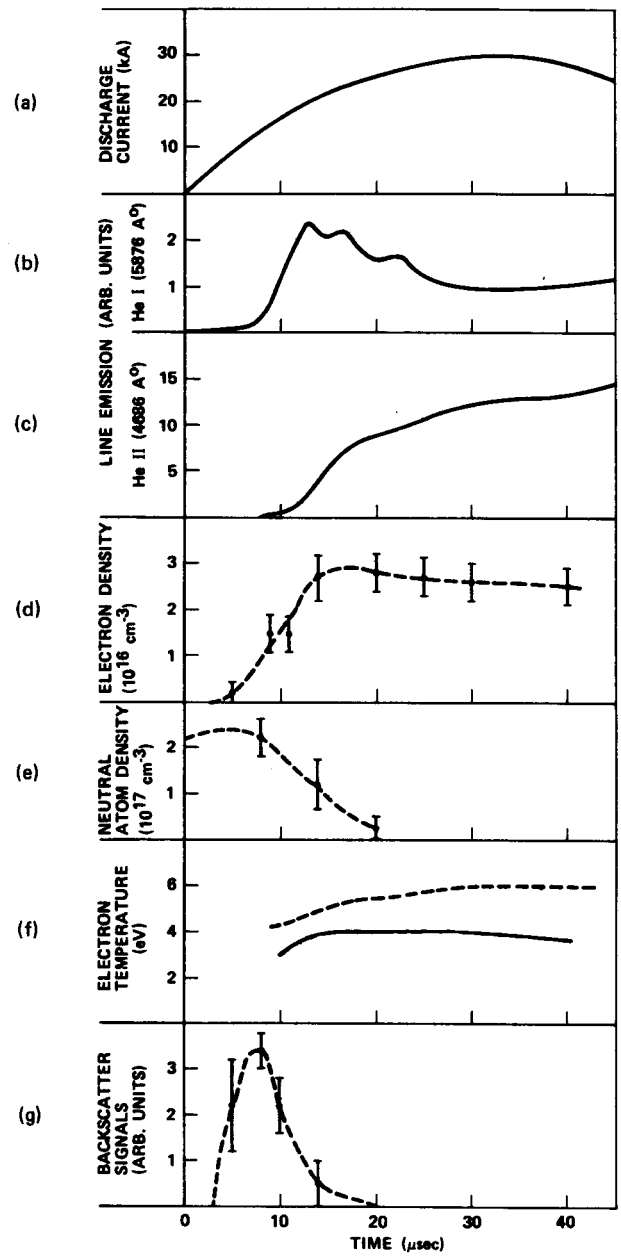

FIG. 2. Typical time history for the pulsed arc helium plasma: (a) discharge current; (b) and (c) on-axis line emission for 5876 Å and 4686 Å, respectively; (d) electron densities measured from linewidths; (e) neutral atom densities from plasma densities attained in the laser focus; (f) electron temperatures from a time-dependent coronal model; and (g) typical backscatter signal magnitudes for different times.

Inferences of electron temperatures were made from the magnitudes and time variation of line intensities assuming a time-dependent, modified coronal model (Ref. 34, Chap. 13). This model has also been referred to as the "collisional-radiative" model,[39] and a brief discussion of the assumptions and techniques of the measurements is given in Ref. 18, Appendix I.

Figure 2 shows a typical time history for the first quarter cycle of the pulsed arc in 7 Torr of helium. The discharge current is shown in (a), while the on-axis emission for the HeI 5876 Å and HeII 4686 Å lines, as viewed end-on, are shown in (b) and (c), respectively. In (d) we have plotted the results of the electron density measurements from the line widths, and in (e) the results for neutral atom densities as inferred from electron densities attained in the laser-heated focal region for laser firings at these times. (Complete outer-shell ionization of the neutrals present in the focus was assumed for these latter measurements.) Analysis of these observations[18] indicates that the possible values for the electron temperature $T_e(t)$ are severely restricted from above by the persistence of neutrals to times as late as $t=10$ μsec, when both the HeI and HeII emissions have begun to rise. We have indicated this upper limit to T_e by the solid line in (f), while the dotted line represents the values of $T_e(t)$ that would be obtained from a *steady-state* coronal model (Ref. 34, p. 274). Note that the conditions implicit in the steady-state model are apparently not attained even at current maximum, when the line emissions have approximately stabilized; Ref. 18 shows that the line intensities must be diffusion-dominated at all times. These observations are consistent with a picture of the plasma in which the active arc region is restricted to the annular volume between the electrode surfaces while the on-axis plasma is produced by diffusion of ions from these current driven regions.

We are now in a position to understand qualitatively the results shown in Fig. 2(g), where we have plotted the observed backscatter signals as a function of time during the discharge. At very early times there is insufficient pre-ionization to prime the breakdown process, and the laser light passes through the neutral gas unabsorbed. At late times ionization and outward diffusion have reduced the neutral density, so that the electron density attained in the focus is only slightly higher than that of the target arc, which is necessarily low because of pressure balance. Only at intermediate times is there a combination of sufficient density of neutrals and priming electrons to produce the highest plasma densities in the focus.

Figure 3 shows typical oscilloscope traces for the HeI 5876 Å and the HeII 4686 Å emissions from the laser heated focus at $t=7$ sec. The width of the 4686 Å line at peak intensity gives a density of 4×10^{17} cm^{-3}. In this case a lower limit on the electron temperature of 25 eV may be inferred from the rate of rise of the HeII emission and the burn-out of the HeI emission.[18] For times after the peak of the HeII emission, estimates of the electron temperature can be made from the instantaneous ratio between the 4686 Å emission

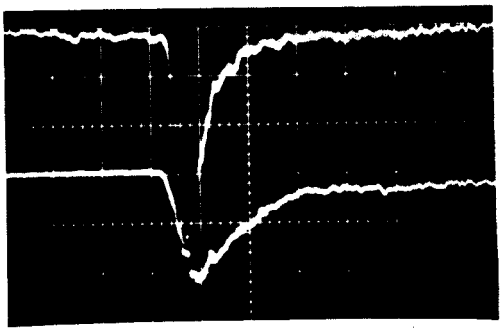

FIG. 3. Typical results for the spectroscopic signals from the laser-heated focus in helium. Upper trace: HeI 5876 Å. Lower trace: HeII 4686 Å. Sweep speed: 200 nsec/div. Signals are inverted.

and the underlying continuum (Ref. 34, p. 283). Unfortunately, the temperature is extremely sensitive to the measured ratio (particularly for small ratios or high temperatures), and there are large uncertainties in the temperatures measured by this method. Furthermore, line emission contributions from the colder ends of the plasma tend to depress the measured temperature somewhat. Nonetheless, from these data we may infer a lower limit on the electron temperature in the focus for helium of about 40 eV, occurring from 0 to 50 nsec after the peak of the 4686 Å emission.

For the other filling gases used, helium was added in small amounts and the line intensities monitored. No essential differences from Fig. 2 were seen in the time histories of the helium lines except for the decrease in intensity expected from the smaller partial pressure of helium. Similarity arguments could then be invoked to presume similar conditions obtained in the arc with these filling gases. Analysis of the time variation of the helium line ratios in the focal regions with helium seeding yielded exactly the same result as for pure helium; i.e., a lower limit on T_e of 25 eV. Unfortunately, the line-to-continuum ratio technique was not applicable in either hydrogen or argon; in the case of hydrogen the ratios become insensitive for much lower values of the temperature, while for argon the indeterminacy in Z_{eff} produces large errors. In the case of argon, however, observations on 4686 Å with helium seeding established a rise in electron density to a value of 5×10^{17} cm^{-3} in 70–90 nsec. Assuming neutral densities no higher than the filling density places several limits on the electron temperature through the ionization rates. In this case we obtain a lower limit for T_e of 80 eV.

In summary, spectroscopic measurements on n_e and T_e were made both in the partially ionized arc plasma and in the fully ionized, laser-heated plasma in the focal region. Data are shown for He only, but similar results were obtained for H_2 and Ar with He seed gas. Densities were best measured by the width of HeII 4686 Å and were of order 2×10^{16} cm^{-3} in the arc plasma and 4×10^{17} cm^{-3} in the heated plasma. Electron temperatures were obtained best from changes in ionization state; these yielded typical lower bounds of 4 eV in the arc plasma and 25 eV in the heated plasma.

B. Probe measurements

A double probe was used in an attempt to measure the density and electron temperature distributions in the arc plasma. Because of the large energy density in the arc, the use of probes was marginal; nonetheless, this diagnostic gave a clear picture of the evolution of plasma density.

The probe tips were tungsten cylinders 0.75 mm in diameter and 1 mm long, separated by 2.1 mm and protruding from alumina tubes. The tips were aligned along the same line of force and then rotationally displaced by their diameter, so as to sample as nearly the same plasma as possible without getting into each other's shadow. Currents as high as 100 A were drawn in densities of order 10^{17} cm^{-3}; consequently, care was taken to minimize the impedance of the leads and of the load. The probe leads from a common probe shaft were connected to separate coaxial cables, which were then connected to each other after passing once around the core of a toroidal current transformer. The secondary of the transformer has 50 turns terminating in a load resistor of 3.9 Ω. The transformer served the double purpose of reducing the effective load to 1.5 mΩ and of rejecting the large common-mode signal from the changing plasma potential. The probe current was supplied by an 80 000 μF capacitor bank.

A saturated ion current could not be obtained because of arcing, but the relative density could be obtained from the probe current at constant bias. Figure 4 shows radial scans of the probe current at various times after firing. From these it is clear that the arc strikes between the tubular electrodes, leaving a weakly ionized region on the axis. The center fills in by diffusion in about 10 μsec. At the early times at which backscattering was observed, the laser-heated region

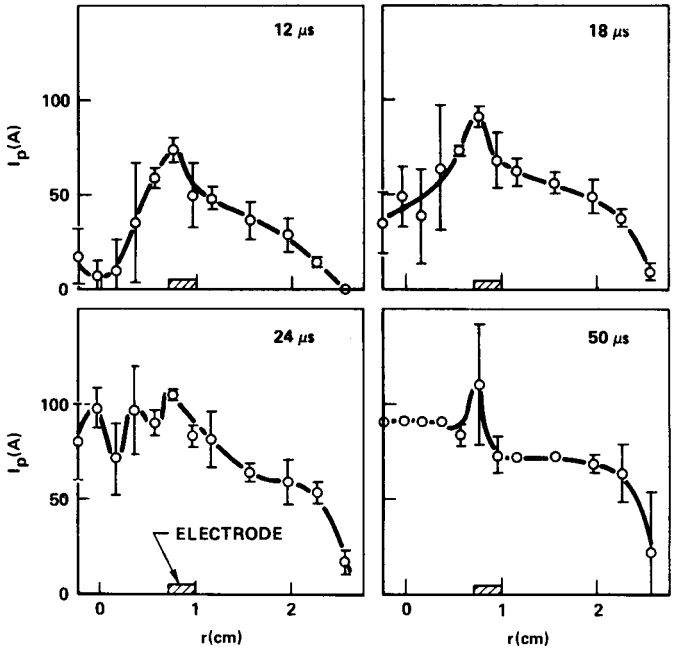

FIG. 4. Radial variation of current to a double probe at constant probe voltage, taken at various times after arc initiation.

was only about 10% ionized, in agreement with the picture obtained from spectroscopy.

V. CALCULATION OF PLASMA EVOLUTION

Despite the desirability of observing backscattering from a preformed and unaltered plasma, it is clear from Sec. II B that laser intensities above threshold will cause significant heating and expansion of the plasma except for extremely short laser pulses. Although the evolution of the plasma under the influence of this heating is a complex interaction of many different processes, these are independently well understood, and their concerted effects should, in principle, be calculable by numerical methods. The specific processes which we have considered are : (1) transfer of the laser energy to the electrons by inverse bremsstrahlung, (2) collisional energy transfer between the electrons and ions, (3) electronic and (4) ionic heat conduction radially outward from the focal volume, (5) hydrodynamic expansion of the laser-heated plasma against the colder background plasma, (6) ionization and recombination between the ion species, and (7) modification of the collisional transport processes to include contributions from multiple ion species, including neutrals.

A number of authors[40-43] have considered different aspects of this problem, particularly including the processes (1)–(5). However, because of the low degree of ionization in the target plasma in our experiment (and others), one expects that processes (6) and (7) may contribute substantially to the time evolution in the focus, particularly for the heavier gases. For example, ionization strongly influences the radial temperature and density distributions, which in turn determine the on-axis temperature through the conductivity.

The computer code utilized a one-dimensional Eulerian mesh scheme with cylindrical symmetry. The code was written specifically so that the various processes could be switched off and the other parameters, such as laser pulse shape and intensity distribution, could easily be modified to make direct comparison with the results of previous calculations by other authors. Specific details concerning the physical model and the calculational scheme are given in Ref. 18, Appendix II.

In Fig. 5 we present the results of a computer run for a test case in hydrogen, with the ionization and recombination processes switched off and the initial conditions and laser characteristics adjusted to match those of the calculations of Burnett and Offenberger.[40] The laser intensity in this case was assumed to have a Gaussian spatial profile with a radius of 175 μm and an approximately triangular time variation with a peak intensity of 6.8×10^{11} W/cm^{-2} occurring at $t=19$ nsec. The calculations of Ref. 40 utilized a Lagrangian mesh which moves with the fluid; the difference between this method and our Eulerian scheme with stationary mesh points is shown by the results. Because the mesh points move with the fluid, the Lagrangian scheme provides the greatest spatial resolution in the vicinity of the shock wave, at the expense of resolution in the regions of lower density. The Eulerian scheme handles

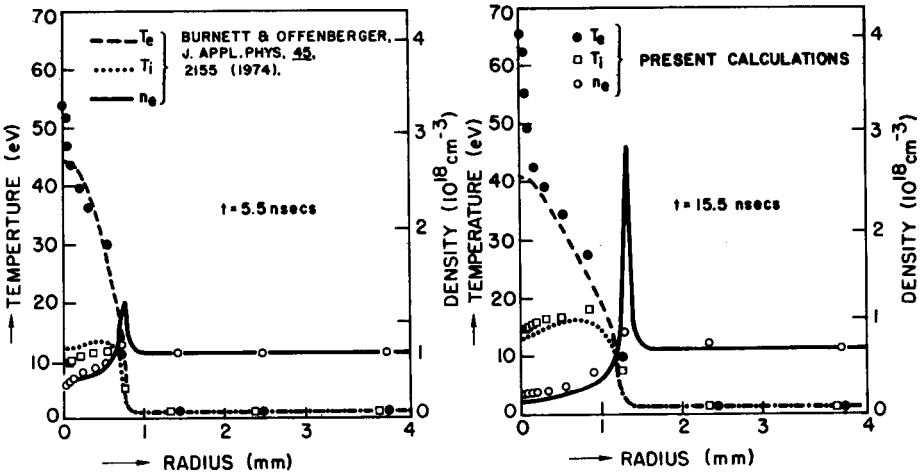

FIG. 5. Calculated radial profiles for n_e, T_e, and T_i at two different times for the test case of the laser intensities and initial plasma conditions considered in Ref. 40. Lines are from data given in Ref. 40, while the data points are the results of the present calculations.

the shock wave in only an approximate fashion but delineates the peak in the electron temperature inside the focus of the laser beam. In the intermediate regions there is excellent agreement.

Having found agreement between our calculations and those of Ref. 40, as well as qualitative agreement with the experiments of Chu and Johnson,[44] we then applied the computer calculations to our experimental conditions with a reasonable degree of confidence. The laser pulse for these latter calculations was assumed to be spatially Gaussian in profile with a radius of 0.35 mm. This gave a peak on-axis intensity of 4×10^{10} W/cm^2. The initial plasma conditions were taken as 5% ionization of the atom densities corresponding to the filling pressure and $T_e = T_i = 1$ eV. The on-axis results of these calculations for the three experimental gases used are plotted in Fig. 6. The lowest plot represents the measured time history of the laser pulse, while above that are shown the results for the electron and ion temperatures and the electron density. In all cases the density peaks slightly before the peak laser intensity, while the electron temperature peaks slightly afterward. This latter result is expected for an on-axis temperature which is only partially heat-conduction limited. The second peak in the electron density for the argon case at approximately 65 nsec results from rapid ionization of the remaining electrons in the outer shell with the rapidly rising temperature.

The increase in density occurring after the peak in the electron temperatures in each case is caused by an implosion phase which appears at late times in all of the calculations. We believe that this is attributable to a characteristic of the calculational scheme. Because of the large bin sizes at the larger radii, the shock wave tended to be dissipated within these larger bins. With the directed energy of the wave dissipated, the density at the position of the wave was free to provide a pressure back inward toward the center of the plasma, causing an implosion. For this reason, the calculations were carried no farther than the density minimum after the peak of the laser pulse. Additionally, variations in the plasma temperature and density of the order of 10% were seen to result from variations in the

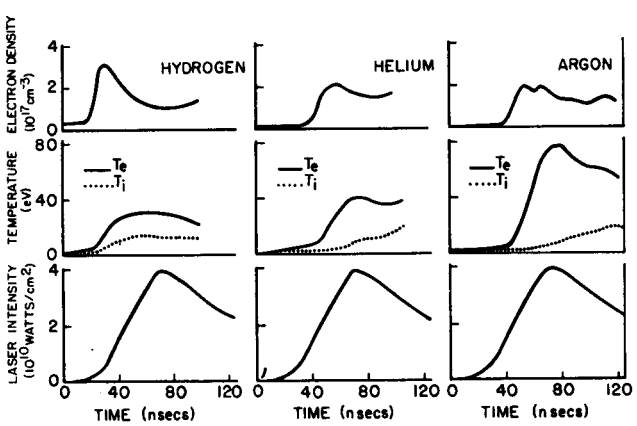

FIG. 6. Calculated time histories of laser heated plasmas for the three gases used in the experiment. Plots represent on-axis values for electron density, electron temperature, ion temperature, and incident laser intensity.

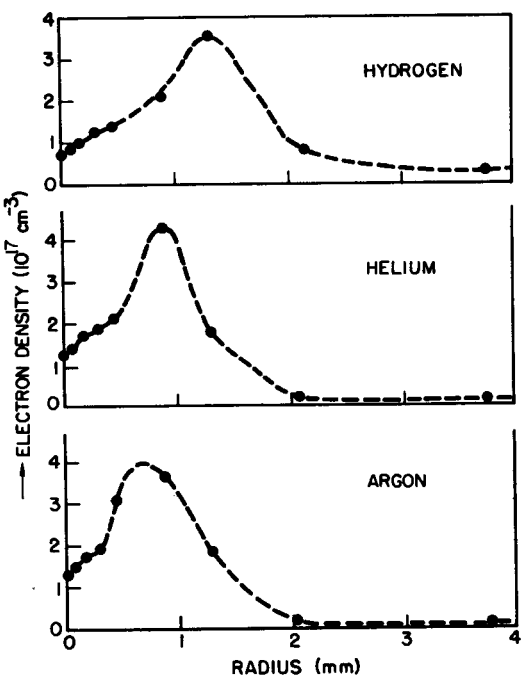

FIG. 7. Computed radial electron density profiles at $t = 80$ nsec, corresponding to the time of the earliest observed backscattering.

mesh placement. Aside from any inadequacies in the model, we must thus expect uncertainties of at least this amount in the calculated results.

A potentially much larger source of error exists, however, in the one-dimensional character of the calculations. Experimentally, we observe refraction effects in the beam transmitted through the plasma which we attribute to sharp density gradients transverse to the direction of propagation, and these are also observed in the computer calculations. In Fig. 7 we have plotted the computed radial electron density profiles obtained at $t=80$ nsec, corresponding approximately to the time of peak electron temperature and the earliest backscatter observations. We see that the strongest gradients occur for the heavier gases due to the slower propagation of the shock wave away from the focal region. Although a proper treatment would involve a two-dimensional calculation including the modification of the beam profile along the axis of the focus, we can obtain a limit on the self-focusing of the beam in these density profiles by using standard formulas[45] for stable propagation of Gaussian beams in parabolic profiles. We then find[18] a radius of 0.1 mm instead of the 0.35 mm assumed in the calculations. However, the focusing length is larger than is available, and only a small reduction in radius can be expected. A factor-of-two increase in I_0 would make our observed threshold agree even better with theory.

VI. BACKSCATTER OBSERVATIONS

A. Qualitative results and backscatter spectra

In Fig. 8 we present typical oscilloscope traces obtained for the backscatter signals. In (a) we show the signal with no plasma in the target chamber, indicating the stray light level and illustrating the shape of the incident laser pulse. The other traces are typical results for various gases and delay times relative to arc firing. In (d) we have increased the sweep speed by a factor of ten to exhibit the backscatter pulses which occur at late times at the higher filling pressures. The backscatter signals appear as a series of very rapidly rising and falling pulses, presumably resulting from backscattering of the individual mode-locked incident pulses. The backscatter signals appeared most reliably just after the peak of the laser intensity, corresponding to the time of peak on-axis temperature in the computer calculations. For the higher filling pressures and the heavier filling gases the backscatter signals tended to move to later times with correspondingly larger jitter and less reproducibility.

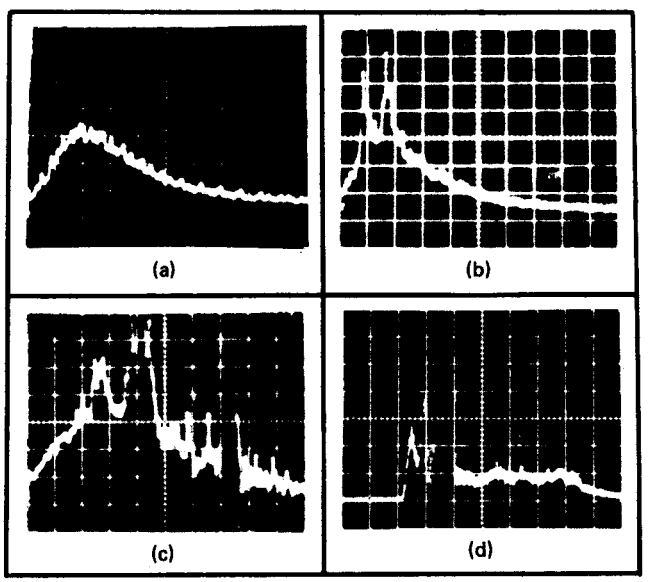

FIG. 8. Typical backscatter signals obtained with (a) stray light only (no plasma); (b) 1.2 Torr argon, $t=5\,\mu$sec; (c) 7.0 Torr helium, $t=7\,\mu$sec; and (d) 8.5 Torr helium, $t=7\,\mu$sec. Sweep speeds are 20 nsec/div in (a)–(c) and 20 nsec/div in (d).

Also seen in the trace in Fig. 8(d) is an enhancement of the stray light level in the tail of the laser pulse which is relatively slowly varying and does not exhibit the spiky nature of the backscatter signals. No frequency shifts were observed for this component. Since it occurred only for the highest densities (filling pressures) and only when strong modifications were seen in the laser beam structure after transmission through the plasma, we ascribe it to refraction effects in the plasma. Although we expect that the plasma should be everywhere underdense, strong density gradients transverse to the beam direction can deflect the beam (for example, into the electrodes) and enhance the stray light level.

In Fig. 9 we present results of Fabry–Perot scans of the backscatter spectrum. The error bars represent the probable error of backscatter signals over 3–5 shots, and the solid lines are corresponding scans of the incident laser spectrum. We see that there is a clear shift of the backscatter spectrum away from the laser frequency. By increasing the free spectral range of the etalon we have established that the shift is to lower frequencies, as expected for stimulated Brillouin scattering.

For an ion acoustic wave with a frequency on the order of 10 GHz and a wavelength of 5.3 μm, one expects, at these plasma densities, that the wave compressions are isothermal for the electrons and one-dimensionally adiabatic for the ions. In the ion wave dispersion relation we may then take $\gamma_e=1$ and $\gamma_i=3$:

$$\omega/k=[(ZT_e+3T_i)/M]^{1/2}. \tag{28}$$

From computer calculations for the time of maximum on-axis electron temperature, we obtain $T_e/T_i=2.5$ for

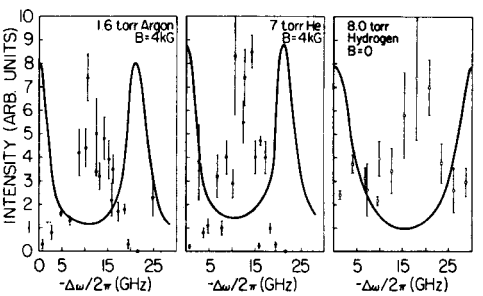

FIG. 9. Spectra of backscattered light in three gases. Solid curves are scans of unshifted stray light. The B values refer to the axial magnetic field of the arc discharge; this had little effect on the experiment.

hydrogen, 3 for helium, and 7 for argon, with effective charge number Z_{eff} equal to 1, 2, and 8, respectively. Inserting values into the dispersion relation together with the wave frequencies obtained from the shifts in Fig. 9 produces values for T_e of 45 eV for hydrogen, 55 eV for helium, and 130 eV for argon.

Among the three gases used, backscattering was seen most easily in argon and least easily in helium in the sense that the backscatter signals persisted longer in argon with decreasing gas pressure. Likewise, the most reproducible signals were seen with argon, although this may be attributable to more uniform preionization with this gas; the most reproducible spectroscopic signals in the pulsed arc were observed with argon.

The backscatter signals plotted in Fig. 9 are for prompt backscatter; that is, for backscatter occurring just after the peak of the laser intensity. Attempts to obtain spectra for the backscatter signals occurring later, primarily at somewhat higher density, proved frustrating. Because of the large error bars, about all that can be said of these spectra is that the frequency shift could be nearly as great as at early times, but could not be determined with precision. However, observations concerning these later backscatter signals were made which helped with interpretation of the data. These are discussed in the next section.

B. Spectroscopic study of later backscatter

Although prompt backscattering signals behaved as expected from the diagnostic measurements and from the model for plasma evolution developed in Sec. V, the presence of backscattering at late times when the laser intensity had decreased by an order of magnitude from its peak value presented some difficulties. Presumably, some new mechanism in the plasma dynamics at these times must be invoked, such as, for example, filamentation or focusing of the laser beam by the plasma profile. In order to study these plasma dynamics, a more detailed investigation of the spectroscopic emissions at late times was undertaken.

For these observations, the two end-on optical channels were modified to improve the spatial resolution in the focus. The magnification of the images of the plasma on the monochromators (see Fig. 1) was increased and the images masked so that only a 200–250 μm diam section of the 1 mm diam focal volume was viewed. With the long optical paths and the magnification (approximately five times) used, focusing and alignment of the two optical channels with the focusing optics of the laser proved to be a challenge. The following procedure was used: A small polished Plexiglass target was inserted into the focal region, and the laser intensity and Ge focusing lens were adjusted until a minimum size burn mark ($\simeq$200 μm) was attained; the burn mark was then illuminated with a cw helium-neon laser, the monochromators set at the position of the 6328 Å laser line, and the focusing and alignment of the optical channels adjusted for maximum response. In this way we were assured that both optical channels viewed the same volume as the infrared backscatter detector. The observations reported here were made in the vicinity of 6500 Å, so that we may reasonably assume that chromatic effects in the optical systems did not alter this alignment.

Utilizing this improved spatial resolution, the features in the accessible spectral region (~3500–7000 Å) were surveyed for characteristics which would provide clues concerning the plasma dynamics at the occurrences of late backscatter. For these surveys the 500-channel analyzer was gated to a 100 nsec period in which late backscatter was most likely to occur, and spectra for shots with and without backscatter were compared. At the same time, the two single-channel detectors were used to monitor the explicit time dependence of the various spectral features. With only one exception to be discussed, no unexpected results were observed. The time histories agreed well with the model of the plasma evolution as developed in the discussion given here. None of the features, save one, exhibited any correlation with the appearance of the backscatter signals.

In Fig. 10 we present typical results for the spectroscopic signals observed for four separate shots with 10 Torr of helium, when the feature monitored was the forbidden 3^1P–2^1P transition of HeI at 6632 Å. As a control, simultaneous traces were taken of the allowed 3^1D–2^1P transition of HeI at 6678 Å, or the continuum emission in the vicinity of 6740 Å. The signals in the two lower traces are inverted and rather noisy due to the low levels of light collected by the optics. The baselines are indicated by markers at the left of the pictures.

First, we should note some differences between the allowed HeI emission shown here [middle traces of Figs. 10(a) and 10(b)] and in Fig. 3. In the previous figure the monochromators were set slightly off line center to reduce the contributions (at line center) from the low density regions at the plasma edge. For the 6678 Å emission of Fig. 10, however, the weak intensity precluded reliable observation of the wings. Observation of the lines used previously in Fig. 2 with this optical system produced essentially the same result as before. In particular, no identifiable structure appears on the time histories of the allowed HeI and HeII lines or of the continuum except for a rise to a peak intensity just after the peak of the laser pulse and subsequent decay. (Note that there is approximately 100 nsec of delay in the optical signals relative to the backscatter signals due to transit times in the photomultiplier tubes.) However, we now wish to consider the forbidden line emission in the bottom traces which shows an extraordinary correlation with the late backscatter signals.

The HeI 3^1P–2^1P transition at 6632 Å is forbidden by the selection rule for electric dipole transitions, which requires a change of parity between the initial and final states, so that for the transiting electron we must have $\Delta l = \pm 1$. The upper 3^1P level lies 104.4 cm^{-1} in energy above the 3^1D level from which arises the corresponding nearby allowed transition at 6678 Å [Fig. 13(a)]. The two upper levels are mixed by the Stark effect so

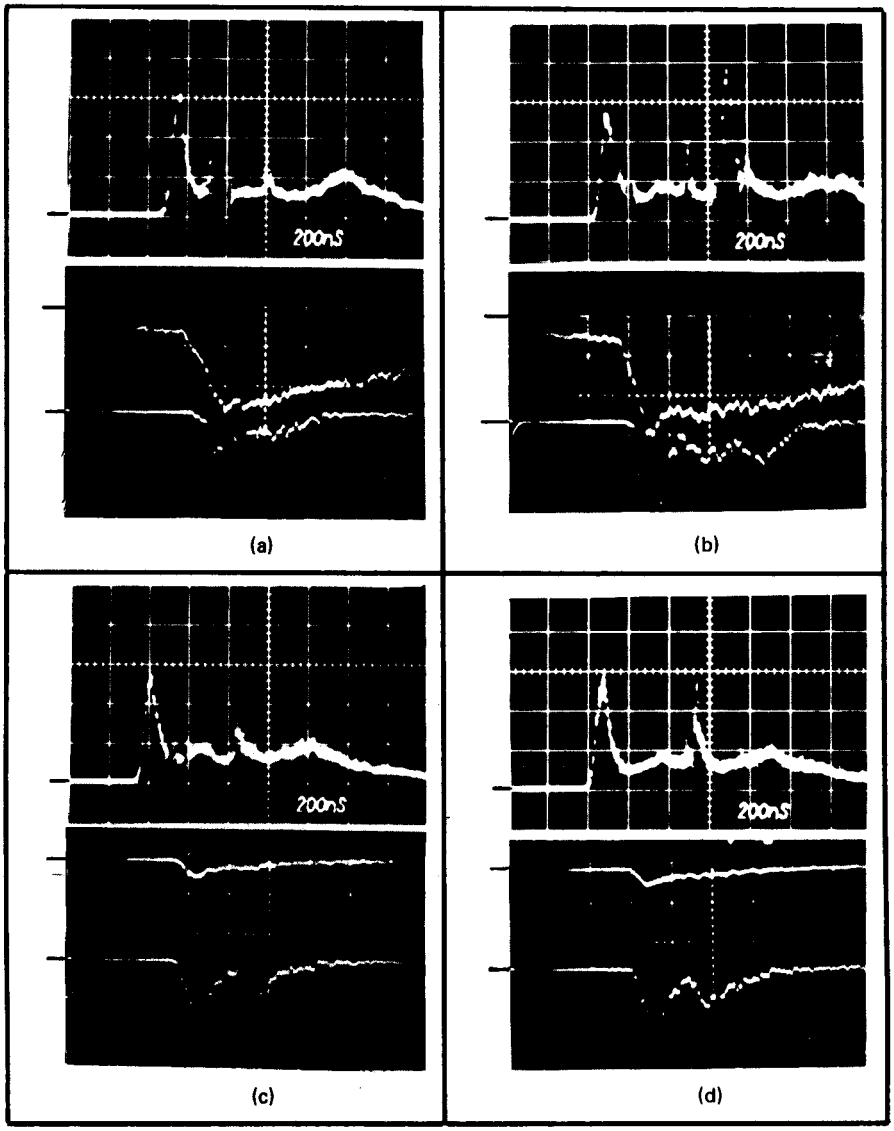

FIG. 10. Correlations between the backscatter signals and the optical emission. Top traces are backscatter signals while the bottom traces are emission from the scattering volume of the HeI forbidden line at 6632 Å. Center traces are the HeI allowed line at 6678 Å in (a) and (b) and the continuum emission near 6740 Å in (c) and (d). Sweep speeds are 200 nsec/div.

that in the presence of an electric field the forbidden line becomes partially allowed. Even in the absence of a wave, the required electric field may be supplied by nearby perturbing electrons and ions, and therefore the forbidden line is sensitive to density. The theory for the resultant density-broadened profiles of the allowed-forbidden line combination has been worked out in detail and shows good agreement with experiment.[46] The initial rise of the forbidden line in Fig. 10, which coincides with the rise of the continuum, we thus attribute to the density rise in the focus. Measurement of the allowed-to-forbidden intensity ratio at this time agrees to within a factor of two with that calculated[47] from the density measured by HeI 5876 Å line broadening. This is within the experimental uncertainty, since complete line profiles of the allowed-forbidden combination in the focus were precluded by the noise. For those shots where no backscatter occurred at late times there was good agreement between the time histories of the forbidden line and the continuum.

As is well known, forbidden line emission can be stimulated by electric fields from other sources, for example, the oscillating electric fields associated with waves traveling within the plasma.[48] In the laboratory, transitions have been observed stimulated by the fields associated with enhanced levels of plasma waves,[49] with microwaves,[50] and with CO_2 lasers.[51] In the theoretical treatment given by Baranger and Mozer,[52] the process is viewed as a second order process involving the emission or absorption of a photon at the frequency of the perturbing field, and the subsequent emission of

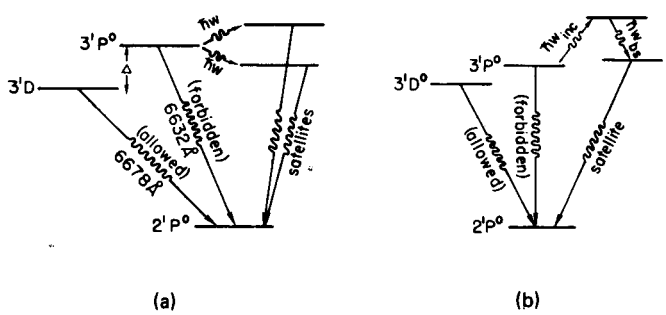

FIG. 11. Energy level diagrams: (a) for the allowed-forbidden combined emission line near 6678 Å in HeI, and for the satellite transitions made possible by an oscillating electric field $\hbar\omega$; (b) for the three-photon satellite transitions.

a photon shifted in frequency from the forbidden line. The transition is then observed by the presence of satellite lines to each side of the forbidden line, displaced by the frequency of the perturbing field [Fig. 11(a)]. The intermediate states in the process are virtual states; that is, they are not allowed by energy conservation, and the atom stays there for only a short time. Using second order time-dependent perturbation theory, Baranger and Mozer calculated that the intensity of these satellites is given by

$$S_s \equiv \frac{R_{II'} h\langle E_\omega^2\rangle}{6m_e^2 e^2(\Delta \pm \omega)^2}, \tag{29}$$

where Δ is the split in angular frequency units between the allowed and forbidden components, ω is the angular frequency of the perturbing electric field, $\langle E_\omega^2\rangle$ is the time average of the field squared, and $R_{II'}$ is a dimensionless radial integral (for the transitions considered here, $\Delta = 2\times10^{13}$ sec^{-1} and $R_{II'} = 40$). The expression Eq. (29) reduces to the usual result for a dc electric field ($\omega = 0$) and may be used theoretically to calculate the line profiles at high density by averaging over the fields of the nearby perturbers. Assuming that the enhanced forbidden-line emission at the time of the late backscatter is attributable to the presence of such field-stimulated satellites, we can calculate the required field intensity from the observed factor-of-two-enhancement over the "steady-state" intensity. The latter is given by I(forbidden) $= 0.02\ I$(allowed), as calculated for our experimental conditions from ordinary Stark effect theory.[47] Taking $S_s = 0.01$, since both satellites are included within our slit width, we obtain, from Eq. (29), the intensity $\langle E_\omega^2\rangle = (96\ \text{kV/cm})^2$.

Experimentally, this interpretation of the forbidden line enhancement provides evidence that the backscattered signals originate from the focal volume and are not due to some less interesting phenomenon such as, for example, the refraction which produces the stray light enhancement in the tail of the laser pulse. The forbidden line enhancement was seen only when the optical systems were accurately aimed at the intensity maximum in the focus of the laser; misalignment by even 250 μm removed the observed enhancement. The high degree of correlation with the time of occurrence of the backscatter signals and the spatial intensity maximum in the focus, as well as the lack of correlation with the other spectroscopic emissions makes implausible any other explanation of the satellite enhancement. It should be noted here that a small increase (<20%) was occasionally observed in the continuum at the times of late backscatter. This increase is probably due to enhanced levels of unidentified satellites; but even if it is attributed to a density rise in a recompression phase of the plasma, such a rise is insufficient to account for the factor-of-two forbidden line enhancement observed. Similar enhancements of the other forbidden lines considered by Baranger and Mozer were not expected to be observable because of masking by other lines or by density broadening, or because of low line intensities; indeed, none was observed.

Unfortunately, as we shall see, some questions still remain as to the source of electric field producing the forbidden line enhancement. The field required is much too large to be the field of the ion wave doing the Brillouin scattering. However, we note for comparison that in the tail of the laser pulse the intensities of the incident and backscattered waves, $I_0 = 5\times10^9$ W/cm^2 and $I_2 = 10^{-6} I_0$, give corresponding field values of $\langle E_0^2\rangle = (435\ \text{kV/cm})^2$ and $\langle E_2^2\rangle = (1.2\ \text{kV/cm})^2$, so that the required field is intermediate to these values. Neither of these fields is individually satisfactory for explaining the enhancement, because in the case of the incident wave the time histories do not match; in the case of the backscattered wave the field is too small; and in both cases the high frequency of the fields would shift the satellites by over 400 Å, well outside our 6.4-Å slit width. One is prompted to look for a nonlinear effect which would mix these fields in the plasma to produce a low frequency field of the right magnitude. To lowest order such a field would be at the beat frequency and have an amplitude proportional to the geometric mean: $(\langle E_0 E_2\rangle)^{1/2} = 23$ kV/cm, and same order as that inferred from the observations. The enhancement in this case would be proportional to the square root of the backscatter power, and something less than a linear dependence is suggested by the traces of Fig. 10. The satellites would be shifted by the beat frequency and therefore not be resolvable here.

Clearly, further work with laser intensities well above threshold is strongly indicated. However, in concluding this section we wish to discuss briefly possible sources for the low-frequency Stark fields. The first is the electric field associated with the ion wave. From the formula for the intensity of the scattered radiation[53]

$$\frac{dI_2}{d\Omega d(\omega/2\pi)} = I_0 V \sigma_T(\theta, \phi) \lim_{T,V\to\infty}\left(\frac{2}{TV}|n_1(k,\omega)|^2\right), \tag{30}$$

we can calculate that the amplitude of the electron density fluctuation associated with the ion wave is $n_1 = 1.7\times10^{-6} n_0$, which in turn corresponds to an ion wave electric field of 1.2 V/cm. Second, the ion wave may be envisioned as being driven by the ponderomotive force arising from gradients in the averaged high-frequency electric field, which in turn, arises from the beat between the incident and backscattered waves.[1] The magnitude of the field corresponding to this force may be written

$$E_{n1} = \frac{e}{m_e\omega_0^2}\nabla\left\langle\frac{E^2}{4}\right\rangle \simeq \frac{e}{m_e\omega_0^2}\frac{\langle E_0 E_2\rangle}{\lambda}, \tag{31}$$

where λ is the wavelength of the interference wave or of the ion wave, giving a field $E_{n1} \simeq 0.05$ V/cm. Neither of these fields is sufficiently large to produce the enhancement.

A nonlinear interaction such as we seek occurs directly in the coupling between the atom and the radiation field through higher order photon processes. We may consider the three photon process in Fig. 11(b) (and similar processes) in which the atom absorbs a photon from the incident laser field, emits one into the backscattered field, and subsequently emits a satellite

photon shifted by the beat frequency. A third-order time-dependent perturbation theory calculation of the transition amplitude for this process yields a sum of terms of the form

$$H^{(1)}_{ij}H^{(1)}_{jk}H^{(1)}_{kl}\,,$$

where $H^{(1)}_{xx}$ are the matrix elements of the interaction Hamiltonian, i is the initial state, l is the final state, and j and k are intermediate states, and, for convenience, we have omitted the usual energy denominators. In the dipole approximation, $H^{(1)}$ has nonzero matrix elements only between states of opposite parity, so that transitions forbidden in first order are likewise forbidden in the third order and all higher odd orders. The amplitude for this process is then zero in the dipole approximation. The contribution from the interaction of the radiation field with higher moments of the atom has already been estimated classically, since from the derivation of the ponderomotive force[54] it is evident (through its dependence on field gradients and first order magnetic effects) that these ponderomotive force contributions are of the same order of magnitude as those from the next higher (quadrupole) moment.

Finally, we consider the possibility that the electron density fluctuation producing the backscattering is due not to an ion wave but to an electron plasma wave; that is, that the late-time backscatter corresponds not to stimulated Brillouin backscattering but to stimulated Raman scattering. In this case the wave oscillation involves a net separation of charge (reflecting the fact that the plasma wave is basically electrical in nature) producing larger electric fields for the same density fluctuations as before. In this case we get a field intensity of $\langle E^2\rangle = (1\ \mathrm{kV/cm})^2$, which is much nearer the right order of magnitude. This interpretation is not inconsistent with our experimental results since we were unable to obtain spectra for the backscatter at these times. Shifts corresponding to densities of the order of 10^{17} cm^{-3} would be displaced several hundred orders on the Fabry–Perot interferometer and would still be within the bandpass of the narrowband filter. In principle, the optical satellite lines would be shifted by approximately 40 Å, which would lie outside the slit width of the monochromator, but because of the large line broadening, an appreciable intensity would still fall within the slit.

We do not expect that the mechanisms considered here exhaust the possibilities. For instance, one could imagine that ion acoustic turbulence might develop during the evolution of the laser-heated plasma disturbance, and that the turbulent fields could both cause forbidden-satellite enhancement and initiate a backscattered wave. A full explanation requires a new experiment; we can only report the remarkable coincidence in space and time of delayed backscatter (presumably Brillouin) and forbidden-line emission.

VII. ANALYSIS AND DISCUSSION OF RESULTS

A. Frequency shift and threshold

The weak backscattered light in this experiment is identified as stimulated Brillouin scattering by its red shift and by the magnitude of the threshold intensity. Other ways to verify the theory of convective parametric instability, such as measuring the slope of the growth curve (reflectivity versus input power), were not possible because the scattering was just above threshold. The use of an $f/20$ focusing lens apparently resulted in such gentle heating of the plasma that the instability started from the thermal level rather than from a high level of ion turbulence, as in other experiments.[9-11]

The measured red shifts are converted to equivalent electron temperatures by means of the ion wave dispersion relation (28) and a calculated T_e/T_i ratio. The results are compared with independent determinations of T_e in Fig. 12 for three gases: H, He, and Ar. The calculated value of T_e takes into account effects not usually considered, such as multiple ionization states and neutral collisions. The measured value of T_e, obtained spectroscopically from the rate of rise of He II 4686 Å, is unfortunately only a lower bound because of limited time resolution. From Fig. 12 one sees that the observed red shifts are in quite good agreement with the expected frequencies of ion waves. Certainly, the scattered light does not come from static ripples, which would give zero shift, or from electron waves, which would give shifts well behond the free spectral range of the Fabry–Perot analyzer. The observed Brillouin red shift appears to be somewhat larger than expected from the computed temperature. This is not unexpected, since there may well be a forward motion of the region doing the scattering.

To compare the observed threshold with theory, we use the formulae given in Sec. II. The number of intensity e foldings above the initial noise level in a length L is given by Eq. (6):

$$N = 2\gamma_0^2 L/c\gamma_s\,. \tag{32}$$

The ion wave damping rate γ_s is found from the dispersion relation

$$Z'(\omega/kv_{\mathrm{thi}}) \simeq (2T_i/ZT_e)(1+k_1^2\lambda_D^2)\,, \tag{33}$$

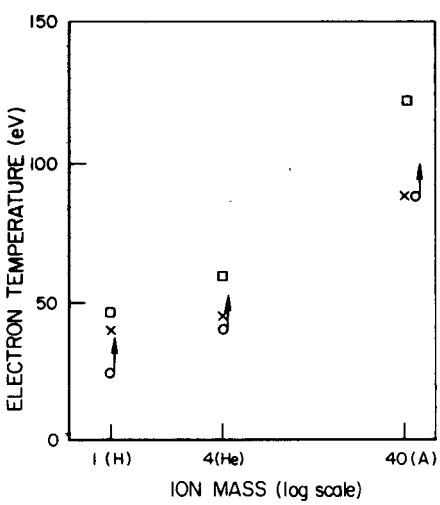

FIG. 12. Comparison of electron temperatures in three gases deduced from backscatter redshifts(□), numerical calculation of plasma evolution (×), and spectroscopy (○). The last is a lower bound only.

where $Z(\zeta)$ is the plasma dispersion function. Although an expansion of $Z'(\zeta)$ in powers of ζ^{-2} does not converge rapidly when T_e/T_i (and hence ζ) is not large, it turns out that the formula of Eq. (34) gives γ_s/ω_s correctly within a factor 2 for T_e/T_i as low as 1.2. Expanding $Z'(\zeta)$ and neglecting $k_1^2\lambda_D^2$ in Eq. (33) we obtain

$$\frac{\gamma_s}{\omega_s} = \left(\frac{\pi}{8}\right)\left(\frac{ZT_e}{T_i}\right)\left(3+\frac{ZT_e}{T_i}\right)^{1/2}\exp\left[-\frac{1}{2}\left(3+\frac{ZT_e}{T_i}\right)\right]. \quad (34)$$

The intensity I_0 required to produce Ne foldings is found found from Eq. (32) with input from Eqs. (1)–(5) and (34). With I_0 expressed in W/cm^2, T_e in eV, n_e in cm^{-3}, and L in cm, this yields the extremely compact result

$$I_0 = 10^{27}(N/L)(T_{eV}/n_e)(se^{-s})^{3/2}\ \mathrm{W/cm^2}, \quad (35)$$

where

$$s \equiv 1+(ZT_e/3T_i) = \tfrac{2}{3}c_s^2/v_{thi}^2. \quad (36)$$

To compare this with observations, we need a value for N, the number of e foldings above thermal noise. For our detector geometry, Thomson scattering from a thermal level of ion waves would give a scattered power of approximately 5 mW into the detector. Since a typical observed value is about 10^4 times this, or 50 W, there are approximately 9 e foldings above thermal. Thus, we let $N=9$. The quiescence of the initial plasma has been verified in a subsequent Thomson scattering experiment.[55] The interaction length L is fixed by the depth of focus, which we take to be $L=3$ cm. The electron temperature is relatively well known from Fig. 12; we take $T_e \simeq 50$ eV for He. For these parameters, the intensity predicted by Eq. (35) for He is shown in Fig. 13 as a function of T_e/T_i encountered during prompt scattering, as taken from the numerical results of Fig. 6. The range of n_e comes from the calculations

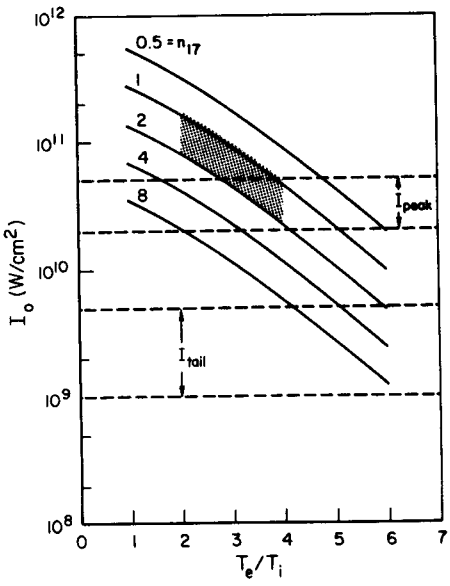

FIG. 13. Theoretical threshold intensity versus temperature ratio for various electron densities n_{17} (in units of 10^{17} cm^{-3}). The curves are drawn for $Z=2$, $T_e=50$ eV, $N=9$, and $L=3$ cm. The ranges of intensities encountered in prompt scattering (I_{peak}) and in delayed scattering (I_{tail}) are shown for comparison. The shaded area represents the experimental parameter range.

(Fig. 6), which give $n_e \simeq 2\times10^{17}$ cm^{-3}, and from spectroscopy (Sec. IV A), which indicates $n_e \simeq 4\times10^{17}$ cm^{-3}. This range determines the range of intensities I_0 required to generate prompt backscatter. The observed intensities I_{peak} are seen to agree well with I_0; the agreement would be better if the effects of self-focusing, neglected here, are included. On the other hand, the intensities occurring in the tail of the pulse are much too low to explain delayed backscatter, especially since T_e/T_i is expected to fall below 2 at late times. Note that prompt scatter is not seen earlier (i.e., before peak intensity) because one must wait for laser heating to lower the threshold by increasing T_e/T_i and decreasing the Landau damping. The exponential term in Eq. (35) gives this effect; the factor T_e/n_e does not vary greatly, inasmuch as both T_e and n_e are increased tenfold by laser heating and ionization.

In summary, the agreement between the predicted and observed threshold intensities shown in Fig. 13 supports the convective theory of stimulated Brillouin scattering, as summarized by Eq. (6). Although several subsequent experiments[9,10,56] have also confirmed this theory, we believe that the present work remains the only one in which stimulated Brillouin scattering is seen to grow from thermal fluctuations in a quiescent plasma.

B. Delayed backscatter

A puzzling feature discovered in this experiment is the occurrence of backscatter during the tail of the CO_2 input pulse, as shown in Fig. 10. The delay from the time of peak intensity varies from 0.2 to over 1 μsec and is typically 0.5 μsec. This is much longer than any obvious time constant in the system. For instance, ion waves excited at laser peak would be damped in approximately 1 nsec, and radial shock waves would transit the focal radius in less than 100 nsec. This eliminates the possibility of a rarefaction wave followed by a recompression, giving a high density at late times. Large T_e/T_i ratios located near laser peak would decay in less than about 10 nsec. The input power in the tail of the pulse is 0.05–0.2 times that at the peak, but because of the weak dependence of T_e on P [Eq. (27)], T_e could be as high as 25 eV there. However, the electron-ion equilibration time is of order 20 nsec at that temperature, and a separation of T_e and T_i cannot be maintained. Thus, not only is I_0 decreased in the tail, but the Brillouin threshold is substantially increased.

We therefore looked for explanations other than stimulated Brillouin scattering for the late signals. Modulation of the laser output by the reflected light would again have too short a characteristic time; furthermore, no irregularities were seen in the stray light signal. Refraction of the beam into a metallic electrode by a high-density arc filament was considered. However, increasing the stray light in this manner would not give the spiky signals characteristic of stimulated Brillouin scatter, as was confirmed by introducing a metal object into the beam. The forbidden-line diagnostic was correlated only with the spiky signals, not the smooth late signals which could indeed be due to

refraction. Although the late scatter could not be frequency analyzed because of poor reproducibility, a spectrum was taken in a subsequent experiment.[57] The late signals were found to be red-shifted.

We found an interesting effect in the high-frequency response of photoconductor detectors such as the Hg:Ge crystal we used. As shown in Ref. 18, the detector is 20 times more sensitive to slow signals than to fast ones at the power levels (~ watts) in question. The response is indeed linear with input power, but the slope of the line is not 1 but 0.85. The same effect has been seen by previous workers,[58] who found the same slope, 0.85, but did not point it out. To check that our delayed signals were not due to a greatly increased sensitivity at late times, we performed a test with a quasi-dc 10.6 μm signal impinging on the detector. It was found that the transition between the low and the high response curves occurred at approximately 50 μsec. This is too long to be applicable to the delayed scatter. The detector effect is still unexplained.

Finally, we discuss two mechanisms for late backscatter that have not been eliminated. One is the formation of a dense ionization front followed by a long region of uniform, heated plasma. The backscatter is seeded by a small amount of dielectric reflection at the sharp front and grows parametrically in the uniform region. This was found to occur in a later experiment[57] with an $f/7.5$ final focus and a radial incidence into the arc column. With $f/20$ and axial incidence an ionization avalanche of this type is not as likely to occur. Spectroscopic observations side-on to the arc column did not show any evidence of moving fronts. Nonetheless, such a front could have formed inside the hollow electrodes, where they could not be seen. Note that the forbidden-line diagnostic does not contradict this possibility because it viewed the entire laser axis. A second mechanism is the formation of a laser-initiated z pinch, giving rise to a filamentary region of hot, dense plasma suitable for Brillouin scatter. The rise time of such a pinch, limited by its inductance, would be approximately 0.25 μsec, which is the right order of magnitude. This hypothesis has neither been proved nor disproved, and the late scatter is still unexplained.

C. Other observations

The remarkable coincidence of forbidden-line emission with delayed backscatter has been discussed in detail in Sec. VI B. The effect is not explained and deserves further study because of its possible value as a diagnostic technique.

The spiky nature of Brillouin scatter seen here and in subsequent experiments is apparently a characteristic of stimulated Brillouin scattering. A number of possible explanations have been offered, but as yet there has been no way to distinguish among them.

Filamentation may be expected to occur along with Brillouin scatter because of the long growth lengths available in this experiment. Indeed, burn paper held at the beam dump often shows a number of small spots indicative of filamentation. However, this did not necessarily occur at the same time or the same axial position as the Brillouin scatter. The effect was not studied in this work.

ACKNOWLEDGMENTS

This work was supported by the U. S. Department of Energy, Division of Laser Fusion, Contract EY-76-S-03-0034, P.A. 236. The cooperation of the Princeton Applied Research Corporation is gratefully acknowledged.

[1]F. F. Chen, in *Laser Interaction and Related Plasma Phenomena*, edited by H. J. Schwarz and H. Hora (Plenum, New York, 1974), Vol. 3A, p. 291.
[2]R. B. White and F. F. Chen, Plasma Phys. **16**, 565 (1974).
[3]C. S. Liu, M. N. Rosenbluth, and R. B. White, Phys. Fluids **17**, 1211 (1974).
[4]J. F. Drake, P. K. Kaw, Y. C. Lee, G. Schmidt, C. S. Liu, and M. N. Rosenbluth, Phys. Fluids **17**, 778 (1974).
[5]D. W. Forslund, J. M. Kindel, and E. L. Lindman, Phys. Fluids **18**, 1002 (1975).
[6]D. W. Forslund, J. M. Kindel, and E. L. Lindman, Phys. Fluids **18**, 1017 (1975); Phys. Rev. Lett. **30**, 739 (1973).
[7]D. W. Phillion, W. L. Kruer, and V. C. Rupert, Phys. Rev. Lett. **39**, 1529 (1977).
[8]J. J. Turechek and F. F. Chen, Phys. Rev. Lett. **36**, 720 (1976).
[9]R. Massey, K. Berggren, and Z. A. Pietrzyk, Phys. Rev. Lett. **36**, 963 (1976); R. S. Massey, Z. A. Pietrzyk, and D. W. Scudder, Phys. Fluids **21**, 396 (1978).
[10]A. A. Offenberger, M. R. Cervenan, A. M. Yam, and A. W. Pasternak, J. Appl. Phys. **47**, 1451 (1976).
[11]F. F. Chen, in *Plasma Physics: Nonlinear Theory and Experiments*, edited by H. Wilhelmsson (Plenum, New York, 1977), p. 82.
[12]D. C. Quimby and L. C. Steinhauer, Phys. Fluids **23**, 1426 (1980).
[13]H. Motz, *The Physics of Laser Fusion* (Academic, New York, 1979).
[14]K. Eidmann and R. Sigel, in *Laser Interaction and Related Plasma Phenomena*, edited by H. J. Schwarz and H. Hora (Plenum, New York, 1974), Vol. 3B, p. 667.
[15]L. M. Goldman, J. Soures, and M. J. Lubin, Phys. Rev. Lett. **31**, 1184 (1973).
[16]W. L. Kruer, E. J. Valeo, and K. G. Estabrook, Phys. Rev. Lett. **35**, 1076 (1975).
[17]B. H. Ripin, F. C. Young, J. A. Stamper, C. M. Armstrong, R. Decoste, E. A. McLean, and S. E. Bodner, Phys. Rev. Lett. **39**, 611 (1977).
[18]J. J. Turechek and F. F. Chen, University of California Report PPG-468 (1980).
[19]M. N. Rosenbluth, Phys. Rev. Lett. **29**, 565 (1972).
[20]C. S. Liu, M. N. Rosenbluth, and R. B. White, Phys. Rev. Lett. **31**, 697 (1973).
[21]D. Pesme, G. Laval, and R. Pellat, Phys. Rev. Lett. **31**, 203 (1973).
[22]D. F. DuBois, D. W. Forslund, and E. A. Williams, Phys. Rev. Lett. **33**, 1013 (1974).
[23]M. N. Rosenbluth, R. B. White, and C. S. Liu, Phys. Rev. Lett. **31**, 1190 (1973).
[24]R. W. Harvey and G. Schmidt, Phys. Fluids **18**, 1395 (1975).
[25]B. I. Cohen and C. E. Max, Phys. Fluids **22**, 1115 (1979).
[26]See, for instance, L. C. Steinhauer, and H. G. Ahlstrom, Phys. Fluids **18**, 541 (1975).
[27]T. W. Johnston and J. M. Dawson, Phys. Fluids **16**, 722 (1973).
[28]M. A. Heald and C. B. Wharton, *Plasma Diagnostics with Microwaves* (R. E. Krieger Publ. Co., Huntington, N. Y.,

1978), 2nd printing, p. 87.
[29]S. I. Braginskii, in *Reviews of Plasma Physics*, edited by M. M. A. Leontovich (Consultants Bureau, New York, 1965), Vol. 1, p. 217.
[30]L. Spitzer, Jr., *Physics of Fully Ionized Gases* (Interscience, New York, 1962), 2nd ed., p. 127.
[31]M. E. Marhic, Phys. Fluids **18**, 837 (1975).
[32]C. Mahn, H. Ringler, and G. Zankl, Z. Naturforsch. A **23**, 867 (1968); H. Wulff, in *Proceedings of the 7th International Conference on Phenomena in Ionized Gases*, edited by B. Perovic and D. Tosic (Gradevinska Knjiga, Beograd, Yugoslavia, 1966), Vol. I, p. 829, and references cited therein.
[33]R. H. Nelson and A. J. Barnard, J. Quant. Spectrosc. Radiat. Transfer **11**, 161 (1971), and references cited therein.
[34]H. R. Griem, *Plasma Spectroscopy* (McGraw–Hill, New York, 1964).
[35]J. Cooper and G. K. Oertel, Phys. Rev. **180**, 286 (1969).
[36]P. C. Kepple, Phys. Rev. A **6**, 1 (1972).
[37]J. J. Turechek, J. Quant. Spectrosc. Radiat. Transfer **16**, 1133 (1976).
[38]H. R. Griem, A. C. Kolb, and K. Y. Shen, Phys. Rev. **116**, 4 (1959) and Naval Research Laboratory Report 5455 (1960).
[39]R. W. P. McWhirter, in *Plasma Diagnostic Techniques*, edited by R. H. Huddlestone and S. L. Leonard (Academic, New York, 1965), Chap. 5.
[40]N. H. Burnett and A. A. Offenberger, J. Appl. Phys. **45**, 2155 (1974).
[41]L. C. Steinhauer and H. G. Ahlstrom, Phys. Fluids **18**, 541 (1975).
[42]S. Y. Yuen, B. Lax, and D. R. Cohn, Phys. Fluids **18**, 829 (1975).
[43]H. A. Bethe and G. C. Vlases, Phys. Fluids **18**, 982 (1975).
[44]T. K. Chu and L. C. Johnson, Phys. Fluids **18**, 1460 (1975).
[45]H. Kogelnik, Appl. Opt. **4**, 1562 (1965).
[46]For example, J. R. Grieg, L. A. Jones, and R. W. Lee, Phys. Rev. A **9**, 44 (1974) and references cited therein.
[47]B. Ya'akobi, E. V. George, G. Bekefi, and R. J. Hawryluk, J. Phys. B **5**, 1017 (1972).
[48]G. Bekefi, Comments Plasma Phys. Controlled Fusion **1**, 9 (1972).
[49]H. J. Kunze and H. R. Griem, Phys. Rev. Lett. **21**, 1048 (1968).
[50]W. S. Cooper, III and H. Ringler, Phys. Rev. **179**, 226 (1969).
[51]D. Prosnitz and E. V. George, Phys. Rev. Lett. **32**, 1282 (1974).
[52]M. Baranger and B. Mozer, Phys. Rev. **123**, 25 (1961).
[53]G. Bekefi, *Radiation Processes in Plasmas* (Wiley, New York, 1967), p. 258.
[54]G. Schmidt, *Physics of High Temperature Plasmas* (Academic, New York, 1966), p. 47ff.
[55]W. A. Peebles and M. J. Herbst, IEEE Trans. Plasma Sci. **PS-6**, 564 (1978).
[56]M. J. Herbst, C. E. Clayton, and F. F. Chen, Phys. Rev. Lett. **43**, 1591 (1979).
[57]M. J. Herbst, C. E. Clayton, W. A. Peebles, and F. F. Chen, Phys. Fluids **23**, 1319 (1980).
[58]T. J. Bridges, T. Y. Chang, and P. K. Cheo, Appl. Phys. Lett. **12**, 297 (1968).